

**Absolute frequency measurement of rubidium 5S-6P transitions**Conny Glaser,<sup>1,\*</sup> Florian Karlewski,<sup>2</sup> Julien Kluge,<sup>3</sup> Jens Grimmel,<sup>1</sup> Manuel Kaiser,<sup>1</sup> Andreas Günther,<sup>1</sup> Helge Hattermann,<sup>1</sup> Markus Krutzik,<sup>3,4</sup> and József Fortágh<sup>1</sup><sup>1</sup>*Center for Quantum Science, Physikalisches Institut, Eberhard Karls Universität Tübingen, Auf der Morgenstelle 14, D-72076 Tübingen, Germany*<sup>2</sup>*HighFinesse GmbH, Wöhrdstraße 4, D-72072 Tübingen, Germany*<sup>3</sup>*Institut für Physik, Humboldt-Universität zu Berlin, Newtonstraße 15, 12489 Berlin, Germany*<sup>4</sup>*Ferdinand-Braun-Institut, Leibniz-Institut für Höchstfrequenztechnik, Gustav-Kirchhoff-Straße 4, 12489 Berlin, Germany*

(Received 17 March 2020; accepted 15 April 2020; published 7 July 2020)

We report on measurements of the 5S-6P rubidium transition frequencies for rubidium isotopes with an absolute uncertainty of  $\leq 20$  kHz for the  $5S \rightarrow 6P_{3/2}$  transition and better than 20 MHz for the  $5S \rightarrow 6P_{1/2}$  transition, achieved by saturated absorption spectroscopy. From the results we derive the hyperfine splitting with an accuracy of 30 kHz and 450 kHz, respectively. This is an improvement of two orders of magnitude for the  $5S \rightarrow 6P_{3/2}$  transition to the current state of the art. We also verify the literature values for the  $5S \rightarrow 6P_{1/2}$  transition, the isotope shifts, as well as the magnetic dipole constants and the electric quadrupole constants.

DOI: [10.1103/PhysRevA.102.012804](https://doi.org/10.1103/PhysRevA.102.012804)**I. INTRODUCTION**

The advent of optical frequency combs has revolutionized the world of high-precision spectroscopy and has enabled measurements of atomic transition frequencies with exceptional accuracy [1–3]. Precise knowledge of these frequencies facilitates better calculations of atomic models and the derivation of more accurate values of physical quantities such as the Lamb shift [4], hyperfine structure constants [5], magnetic dipole or electric quadrupole constants. Furthermore, accurate values are desirable to experimentally investigate novel ways of manipulating atomic states, such as the coherent excitation of Rydberg atoms for quantum information processing [6,7], generation of atomic memories [8], or implementing novel quantum gates [9].

For quantum information purposes rubidium Rydberg atoms are a widely used species. A common way to excite rubidium atoms from the 5S ground state to Rydberg states with high principal quantum numbers  $n$  is via a three-level ladder scheme  $5S \rightarrow 5P \rightarrow nS$  or  $nD$  using a pair of lasers with wavelengths 780 nm and 480 nm. This scheme, however, commonly relies on the generation of 480 nm light by frequency doubling a 960 nm laser [10], which limits the available laser power. Also, second harmonic generation setups are much more complicated than single diode emitters.

A promising alternative is the excitation using the 6P state as intermediate state [11,12]. Due to the five times longer lifetime  $\tau = 121$  ns compared to the 5P state [13], dephasing during the excitation is reduced and the coherence times resulting from this transition are expected to be larger [9,14]. The commercial availability of 420 nm external cavity diode lasers (ECDL) renders the Rydberg excitation (ladder) scheme via the 6P intermediate state a viable alternative to

the commonly used excitation state via the 5P state. Additionally, the light driving the  $6P \rightarrow nS$  transition at 1016 nm can easily be generated with high power using ECDLs and allows high Rabi frequencies for the excitation to Rydberg states. Moreover the dipole matrix elements are larger for this transition.

While the transition frequencies for the excitation scheme  $5S \rightarrow 5P$  are known to 6 kHz accuracy [15], there has been so far no absolute data available for the transition  $5S \rightarrow 6P$ ,  $6P \rightarrow nS$ ,  $nD$ , which is, however, necessary for the implementation of quantum information protocols using this excitation path. Knowing the 6P transition frequencies and the fine and hyperfine structure sublevels with high accuracy, the transition frequencies from the 6P intermediate state to Rydberg states can then be calculated using quantum defect theory [10,16–18]. Measurements of the hyperfine splitting of the <sup>85</sup>Rb and <sup>87</sup>Rb 6P levels have been performed before [19], but the most accurate value for the absolute frequencies for  $6P_{3/2}$  in literature have uncertainties of 6 MHz [20].

Here, we report on the measurements of the absolute frequencies for these transitions and on measurement schemes to determine the relative frequencies. We have measured the absolute frequencies of the  $5S \rightarrow 6P_{3/2}$  resonance with an uncertainty of  $\leq 20$  kHz and  $\leq 20$  MHz for the  $5S \rightarrow 6P_{1/2}$  transition. The improved accuracy of the  $5S \rightarrow 6P_{3/2}$  resonance is due to the use of a narrow linewidth frequency comb, while the frequencies of the other transition are based on a measurement using a wavelength meter. This improves the aforementioned literature values for the  $5S \rightarrow 6P_{3/2}$  transition [20] by two orders of magnitude. In addition to these measurements we verify the literature values of the isotope shifts [21,22], the magnetic dipole and electric quadrupole constants [19], and have also determined the hyperfine splittings, depicted in Fig. 1, from the measured transition frequencies, which brings their accuracies to the same respective orders of magnitude.

\*conny.glaser@uni-tuebingen.de

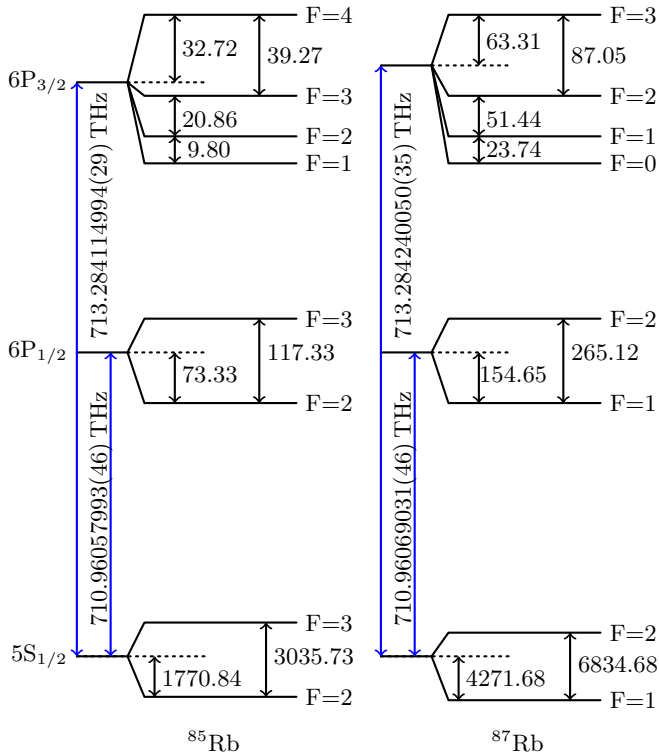


FIG. 1. Level scheme and hyperfine splitting (rounded, in MHz) for the  $5S_{1/2}$  and  $6P$  manifold of  $^{85}\text{Rb}$  (left) and  $^{87}\text{Rb}$  (right). For the exact values of the  $6P_{1/2}$  and  $6P_{3/2}$  hyperfine splitting see Table III. Drawing not to scale.

## II. EXPERIMENTAL SETUP

Our experimental setup is a saturation spectroscopy as shown in Fig. 2. The laser source is an ECDL with a linewidth of  $<400$  kHz as measured by the beating signal between the ECDL laser and the frequency comb. The frequency comb is phase locked to a 1550 nm fiber laser (X15, NKT) with a linewidth of  $<100$  Hz.

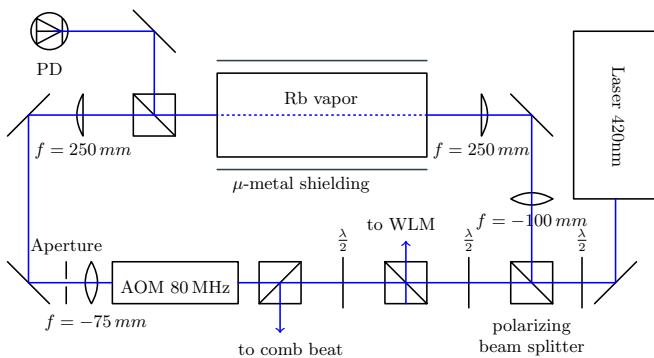


FIG. 2. Optical setup for the measurement of the  $5S \rightarrow 6P$  transitions in a rubidium vapor cell. The probe and pump beams are counter propagating in the cell (heated to  $\approx 321$  K). The probe laser intensity is monitored with a photodiode (PD) and the pump beam is chopped with an 80-MHz acousto-optic modulator (AOM). Both beams originate from an external cavity diode laser, which is either scanned by a wavelength meter (WLM) ( $5S \rightarrow 6P_{1/2}$  transition) or locked to the frequency comb ( $5S \rightarrow 6P_{3/2}$  transition).

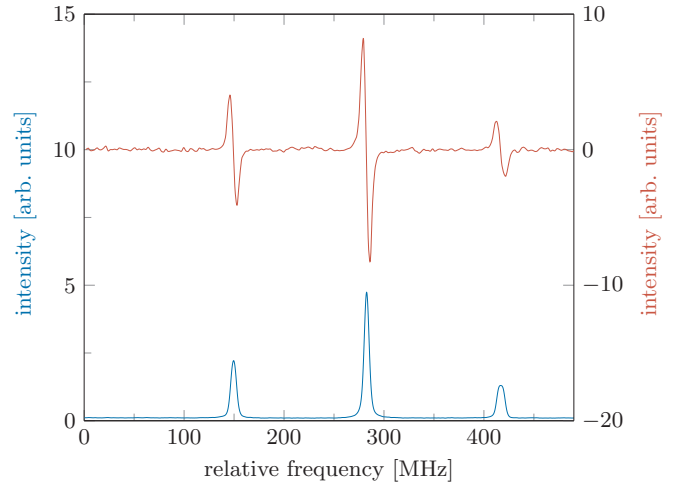


FIG. 3. Doppler free spectrum (blue, bottom) and the resulting error signals (red, top) for the  $^{87}\text{Rb}$   $5S_{1/2}$  ( $F=1$ )  $\rightarrow$   $6P_{1/2}$  transitions.

The pump and probe beams counterpropagate through the heated rubidium vapor cell (321 K), with a length of 10 cm and a diameter of 2 cm. Both laser beams are enlarged via lenses to illuminate a wide area within the cell. Polarizing beam splitters ensure crossed linear polarizations to avoid interference effects within the cell. A double-layer magnetic  $\mu$ -metal shielding leads to a reduction of magnetic fields.

The power ratio between probe and pump beams is adjusted in order to optimize the signal-to-noise ratio of the Lamb dips. The optimal ratio is found to be near (10:1), using a probe power of 0.488 mW ( $I_{\text{max}} = 14.9$  mW/cm<sup>2</sup>) and a pump beam power of 56  $\mu$ W ( $I_{\text{max}} = 1.2$  mW/cm<sup>2</sup>). The intensity and the frequency of the pump beam are modulated with a frequency of 50 kHz using an 80 MHz acousto-optic modulator (AOM). The probe beam signal from the photodiode is subsequently demodulated at the same frequency using a lock-in amplifier (HF2LI, Zurich Instruments), which results in a fully Doppler free spectroscopy signal [23], as depicted exemplarily in Fig. 3 (blue line) for the  $^{87}\text{Rb}$   $5S_{1/2}$  ( $F=1$ )  $\rightarrow$   $6P_{1/2}$  ( $F'=1$ ) transitions. Since the AOM shifts the pump beam by 80 MHz the measured Lamb dips and crossovers are red shifted by  $-40$  MHz. This offset is corrected in the final data analysis.

The relative frequencies between the  $5S \rightarrow 6P_{1/2}$  transitions are measured by scanning the laser with a wavelength meter (WS8-2, HighFinesse) and simultaneously recording the wavelength of the laser. Additionally, we can impose 3 MHz sidebands by frequency modulation (FM) of the laser diode current. After appropriate demodulation, this leads to a Pound-Drever-Hall-like (PDH) error signal, which can be used to stabilize the laser onto the transition resonance frequency [24]. Figure 3 shows an exemplary spectrum acquired by the lock-in amplifier (blue) and the FM error signals (red) for the  $^{87}\text{Rb}$   $5S_{1/2}$  ( $F=1$ )  $\rightarrow$   $6P_{1/2}$  transitions.

We can control the frequency of the laser in three ways. The first is to stabilize the laser frequency with the FM

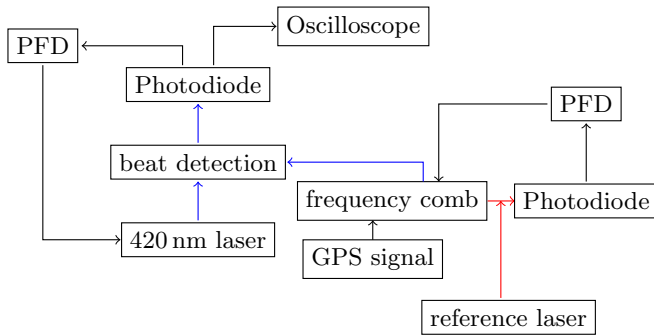


FIG. 4. Block diagram of the locking scheme for the 420 nm laser and the frequency comb. The modes of the comb, locked to a RF reference, and the light of a narrow linewidth 1550 nm laser are superimposed and monitored on a photodiode. Using the beating signal the comb is phase locked with a phase frequency detector (PFD). The 420 nm laser is in the same way phase locked to the frequency comb and the beating signal is acquired with a digital oscilloscope.

error signal to one of the transitions using a digital laser locking module (DigiLock, Toptica). Alternatively, the laser frequency can be stabilized and scanned by the wavelength meter, which is calibrated with a laser that is frequency stabilized to the  $5S_{1/2}(F=2) \rightarrow 5P_{3/2}(F'=3)$  transition of  $^{87}\text{Rb}$  (780.246291 nm) via a FM spectroscopy. Those methods are used to measure the absolute and the relative frequencies for both transitions. For the third method the beam of the ECDL and the modes of a narrow linewidth frequency comb (Toptica) are superimposed and frequency filtered by a grating in a beat detection unit (DFC BC and DFC MD, Toptica) and monitored on a photodetector with a bandwidth of 50 MHz. The resulting beating signal is acquired with a digital oscilloscope (Picoscope 5442A, Pico Technology). Using the beating signal the 420 nm laser is phase locked to the frequency comb, using a phase frequency detector (PFD, Toptica) with a filter, that is tunable between 2 and 38 MHz (cf. Fig. 4) and a fast laser locking module (FALC, Toptica). A typical phase-locked beating signal with a width of  $\approx 1$  kHz can be seen in Fig. 5. An offset-free narrow linewidth frequency comb with a repetition rate of  $f_{\text{rep}} = 80$  MHz serves as a frequency reference for the laser. The comb linewidth below 5 kHz is achieved by phase locking the comb to an ultralow noise fiber laser using a phase frequency detector and a fast laser locking module. The laser frequency is stabilized with the error signal of a radio frequency reference with an accuracy of  $\leq 2 \times 10^{-11}$  and the repetition rate of the frequency comb. The long-term frequency accuracy is better than 2 kHz. The comb's linewidth is measured by a beating of the comb with a free running narrow linewidth NKT laser, the absolute frequency is measured by comparing it to a second frequency comb (FC 1500, Menlo).

This method to measure the frequencies is only applicable to the  $5S \rightarrow 6P_{3/2}$  transition since the comb does not support the corresponding wavelength to the  $5S \rightarrow 6P_{1/2}$  transition. Figure 6 shows a typical saturation spectrum for the  $5S \rightarrow 6P_{3/2}$  transition.

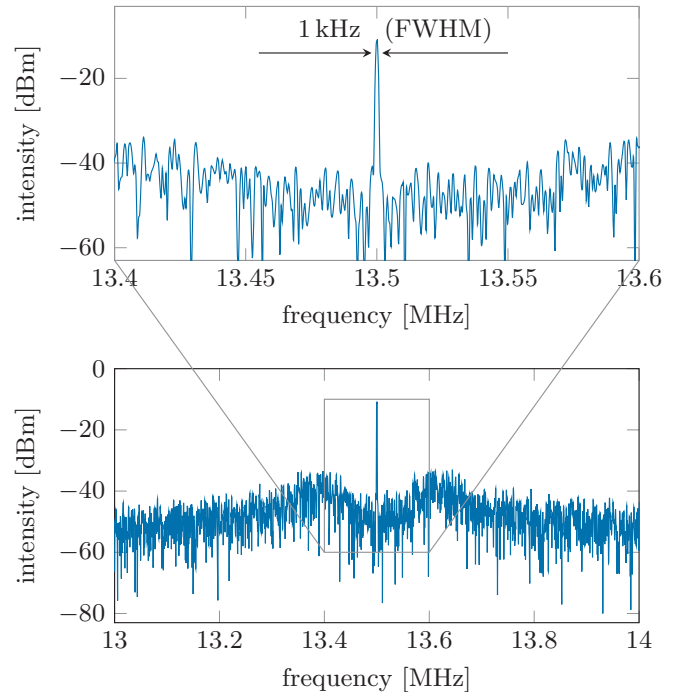


FIG. 5. Typical phase-locked beating signal between the 420 nm laser and a narrow line frequency comb. The top graph is a zoom into the region of the beating signal, showing a width of  $\approx 1$  kHz.

### III. MEASUREMENT OF THE $5S \rightarrow 6P_{3/2}$ TRANSITIONS

For the measurement of the absolute transition frequencies the ECDL laser is beaten with the frequency comb. The laser is locked to the FM error signal of each transition. Simultaneously, the wavelength meter records the frequency and a digital oscilloscope saves the beat frequency. Knowing these values and the repetition rate of the comb, we are not only able to determine the related comb mode but also to calculate the absolute frequencies. In order to reduce the statistical error, each measurement is repeated 60 times and subsequently

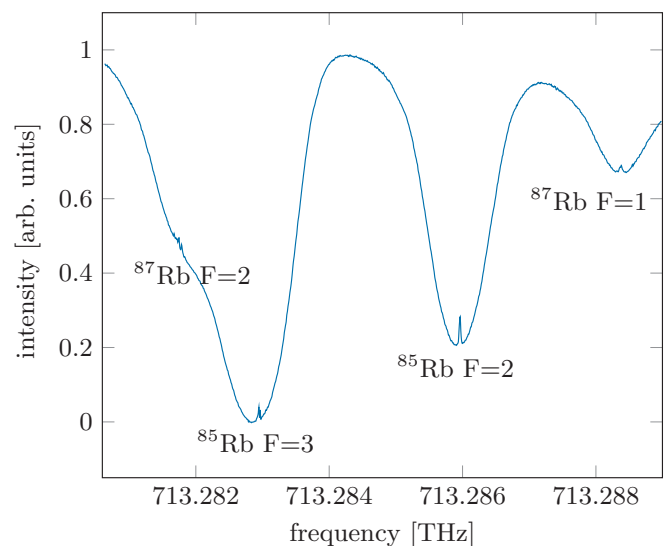


FIG. 6. Saturation spectrum for the  $5S \rightarrow 6P_{3/2}$  transitions for  $^{85}\text{Rb}$  (inner dips) and  $^{87}\text{Rb}$  (outer dips).

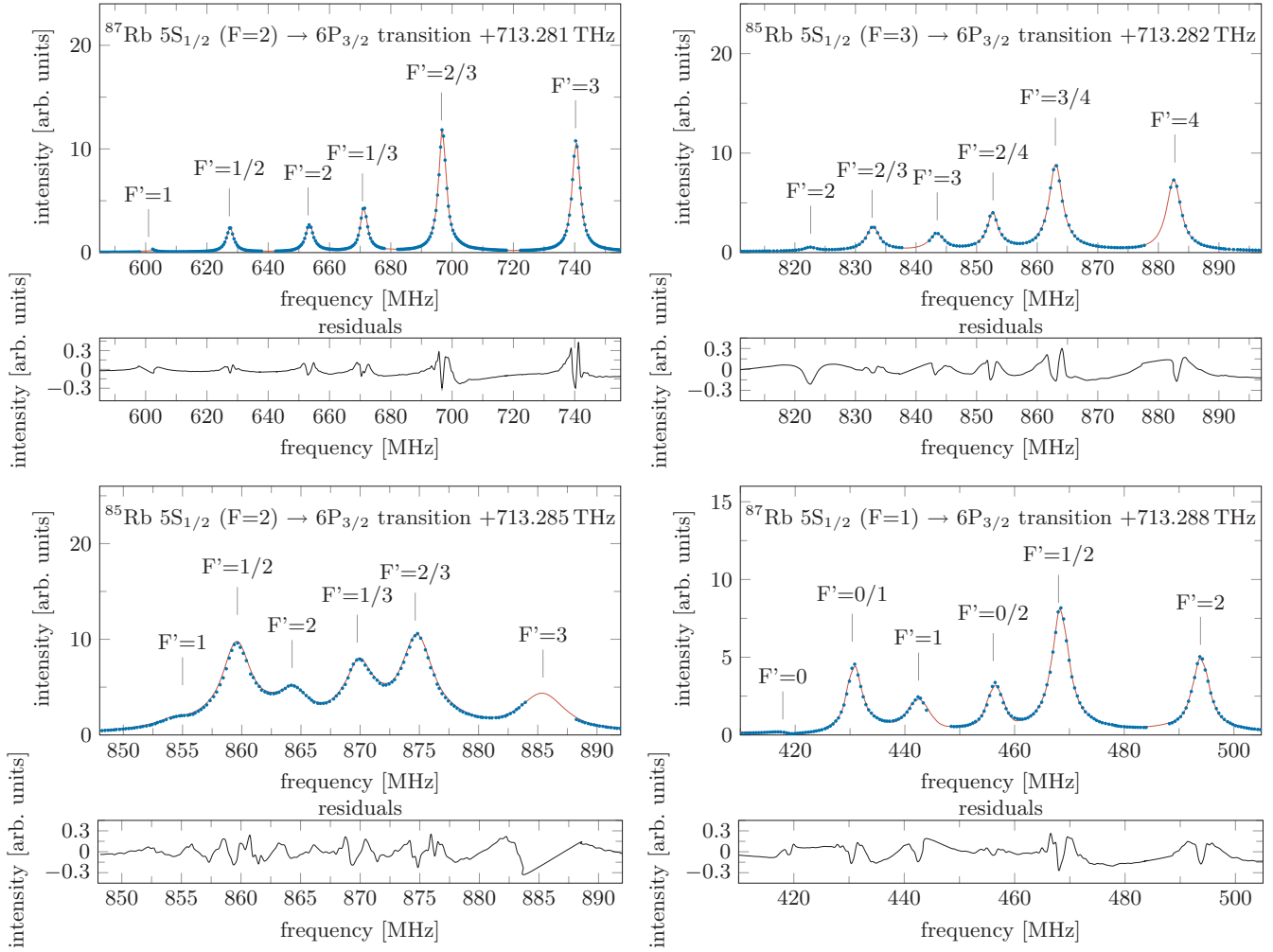


FIG. 7. Recorded spectra (blue dots) and fitted superpositions of Voigt functions (red solid line) for the  $5S_{1/2} \rightarrow 6P_{3/2}$  transition. The gaps in the spectra are caused by the PFD locking scheme, which can only be tuned between 2 and 38 MHz for each comb mode, resulting in 4 MHz gaps whenever the comb mode has to be changed. Below each spectrum the residuals are shown.

averaged. To characterize the long-term locking accuracy, we lock the 420 nm laser to an arbitrary frequency for 1 h and record the beating signal between laser and frequency comb every 15 s. We find that in one hour the lock frequency of the laser deviates less than 11.6 kHz (FWHM) from its mean value.

The relative frequencies are set by locking the laser to the frequency comb at a given locking point using the PFD. Starting at the previously measured frequencies and scanning this locking point between 2 and 38 MHz for the corresponding comb mode, the relative frequencies to the  $5S_{1/2} \rightarrow 6P_{3/2}$  transitions can be determined with an accuracy of  $\leq 2$  kHz resulting from the comb uncertainty. Figure 7 shows the resulting spectra from these scans, which have been calibrated using the absolute frequencies from the wavelength meter measurement. The gaps in the measured spectra are caused by the locking scheme with the PFD, which can only be tuned between 2 and 38 MHz for each comb mode, since there has to be a frequency difference to the next comb mode. This results in 4 MHz gaps whenever the comb mode has to be changed.

For each isotope and set of transitions starting from the same hyperfine ground state the spectrum is fitted using a superposition of six Voigt profiles. From this fit we determine the transition frequency, the width of both Gaussian and Lorentzian curve, and the amplitude of each of the six peaks within one set of transitions. This yields line widths of  $\approx 2.7$  MHz (FWHM), roughly twice as large as expected from the natural linewidth of 1.416 MHz [25]. The  $2\sigma$  uncertainties arising from the fit routine were calculated separately for each spectrum and are found to be smaller than 19 kHz.

The uncertainty in the data for the absolute frequency comprises several known error sources such as the laser linewidth uncertainty of the phase-locked laser ( $\leq 2$  kHz) and technical noise. Additionally, the fitting error contributes to the uncertainty of the measured frequency. The overall  $2\sigma$  uncertainty resulting from these effects was determined independently for each measured transition and is found to be  $\leq 20$  kHz. The absolute transition frequencies and the corresponding  $2\sigma$  uncertainties are summarized in Table I.

TABLE I. Measured absolute transition frequencies between the  $5S_{1/2}$  and  $6P_{3/2}$  states of  $^{85}\text{Rb}$  and  $^{87}\text{Rb}$ .  $2\sigma$  uncertainties are given in brackets.

	Transition	Frequency [THz]
$^{87}\text{Rb}$	$F = 2 \rightarrow F' = 1$	713.281601856(16)
	$F = 2 \rightarrow F' = 1/2$	713.281627578(16)
	$F = 2 \rightarrow F' = 2$	713.281653300(16)
	$F = 2 \rightarrow F' = 1/3$	713.281671103(16)
	$F = 2 \rightarrow F' = 2/3$	713.281696825(16)
$^{85}\text{Rb}$	$F = 2 \rightarrow F' = 3$	713.281740350(16)
	$F = 3 \rightarrow F' = 2$	713.282822710(16)
	$F = 3 \rightarrow F' = 2/3$	713.282833135(16)
	$F = 3 \rightarrow F' = 3$	713.282843560(16)
	$F = 3 \rightarrow F' = 2/4$	713.282852768(16)
	$F = 3 \rightarrow F' = 3/4$	713.282863193(16)
$^{85}\text{Rb}$	$F = 3 \rightarrow F' = 4$	713.282882825(16)
	$F = 2 \rightarrow F' = 1$	713.285848620(18)
	$F = 2 \rightarrow F' = 1/2$	713.285853521(18)
	$F = 2 \rightarrow F' = 2$	713.285858422(18)
	$F = 2 \rightarrow F' = 1/3$	713.285863949(18)
	$F = 2 \rightarrow F' = 2/3$	713.285868850(18)
$^{87}\text{Rb}$	$F = 2 \rightarrow F' = 3$	713.285879278(18)
	$F = 1 \rightarrow F' = 0$	713.288412811(20)
	$F = 1 \rightarrow F' = 0/1$	713.288424683(20)
	$F = 1 \rightarrow F' = 1$	713.288436555(20)
	$F = 1 \rightarrow F' = 0/2$	713.288450406(20)
	$F = 1 \rightarrow F' = 1/2$	713.288462278(20)
	$F = 1 \rightarrow F' = 2$	713.288488000(20)

We also perform measurements of the absolute transition spectra using the wavelength meter to lock the laser. The experimental sequence is as follows: First, the wavelength meter is calibrated as described above. Second, the laser frequency is swept linearly at a rate of 50 MHz/s over a range of 250 MHz while the signal of the lock-in amplifier was recorded. In order to reduce the statistical error, each trace is measured 100 times and then averaged. The deviations between this measurement and the one including the frequency comb is found to be smaller than 500 kHz (FWHM).

#### IV. MEASUREMENT OF THE $5S \rightarrow 6P_{1/2}$ TRANSITIONS

Since the output of the frequency comb near 420 nm is limited to a range between 418.8 nm and 420.3 nm it is not possible to obtain sufficient beating signals for the  $5S_{1/2} \rightarrow 6P_{1/2}$  transition at 421 nm. Therefore, the frequency measurements for this manifold are based on the DigiLock module and wavelength meter scans. With the wavelength meter calibrated at 780 nm, the  $2\sigma$  uncertainty at 421 nm amounts  $\leq 20$  MHz [26].

Similarly, as described above, the frequencies are determined by locking the laser to the error signal using the DigiLock. Then the laser is locked to a calibrated wavelength meter and swept at a rate of 50 MHz/s over a range of 500 MHz to measure the spectra. Again, each trace is measured 100 times and subsequently averaged, to reduce

statistical errors. The resulting spectra are depicted in Fig. 8. Compared to the expected linewidth of 1.299 MHz [25], we typically measure line widths (FWHM) of  $\approx 2.8$  MHz. The positions of the peaks are evaluated by fitting superpositions of Voigt profiles to the spectra. The  $2\sigma$  uncertainty due to the fitting routine is on the order of a few kHz. This and the deviations due to the linewidth of the laser can be neglected compared to the absolute uncertainty of the wavelength meter. The results for the transition frequencies and their absolute  $2\sigma$  uncertainties are summarized in Table II.

To estimate the relative uncertainty caused by the wavelength meter we characterize its locking accuracy. Therefore we lock the 420 nm laser to an arbitrary frequency within the output range of the frequency comb for 1 h and record the beat signal between laser and a frequency comb mode every 15 s. We find the frequency of the calibrated wavelength meter to be normally distributed with a  $2\sigma$  uncertainty of 320 kHz. The relative  $2\sigma$  uncertainty is calculated to be 470 kHz combining the laser linewidth of  $< 400$  kHz and the relative uncertainty of the calibrated wavelength meter.

#### V. DISCUSSION

To determine the influence of cell and other residual shifts we additionally performed the measurement with the laser locked to the frequency comb for the  $5S_{1/2}F = 2 \rightarrow 5P_{3/2}F = 2/3$  crossover and found the difference between the theoretical value [15] and the fit to the data being less than the fitting uncertainties.

Since pressure broadening is negligible ( $< 1$  kHz) the broadening of the natural linewidth is assumed to be mostly the consequence of the transversal Doppler effect ( $1 \text{ MHz}/0.12^\circ$ ). Lowering the power of the lasers did not influence the line widths. In Table II we compare our measurements with the results of Ref. [27]. Our mean values deviate by about 5 MHz from the literature values, which is well within the estimated wavelength meter uncertainty. While the absolute uncertainty of the wavelength meter dominates the error bars for the transition frequencies, the relative uncertainty holds regarding the following considerations.

The hyperfine splitting values in Table III are the differences between matching pairs of transitions from Table I for the  $5S \rightarrow 6P_{3/2}$  transitions and Table II for the  $5S \rightarrow 6P_{1/2}$  transitions. The  $2\sigma$  uncertainties are calculated via error propagation based on the transition frequency uncertainties. For a comparison to the results from Ref. [19] we have calculated the hyperfine splittings from their given values of the magnetic dipole constant  $A$  and the electric quadrupole moment  $B$ . Table III shows a comparison between these values derived from the literature and the values determined from our experimental spectra, which are in good agreement. As depicted in Fig. 1 we also calculated the hyperfine shifts and the transition frequencies from the ground state to the  $6P_{1/2}$  and  $6P_{3/2}$  state, respectively.

With those splitting values, the magnetic dipole constant  $A$  and the electric quadrupole constant  $B$  can be calculated. This was accomplished by first evaluating the frequency differences between all possible combinations of hyperfine

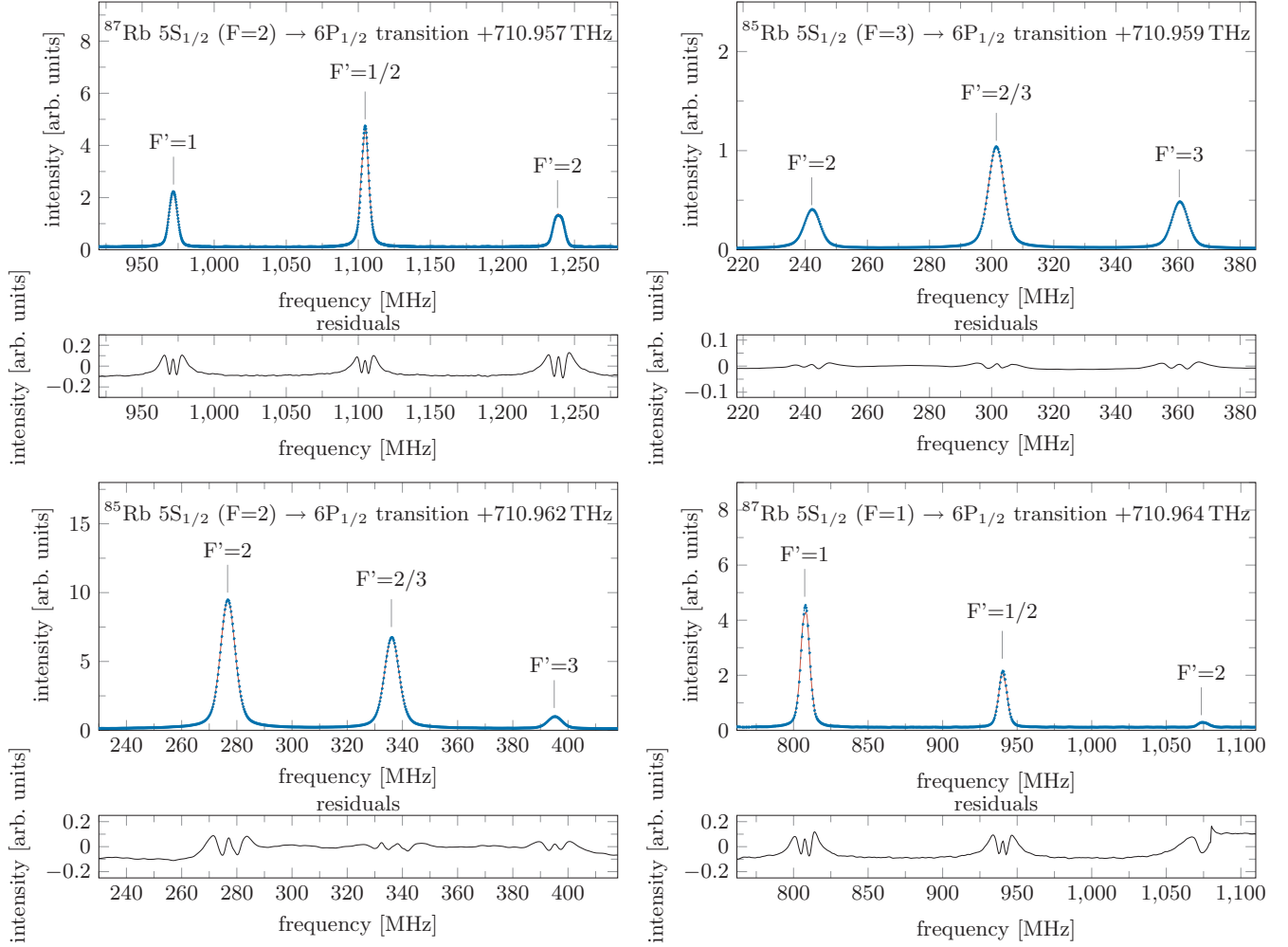


FIG. 8. Recorded spectra (blue dots) and fitted superpositions of Voigt functions (red solid line) for the  $5S_{1/2} \rightarrow 6P_{1/2}$  transitions. Below each spectrum the residuals are shown.

substates. Full error propagation with the previously obtained correlations were performed and used in a linear least-square minimization of the form  $A f_1(F, F') + B f_2(F, F')$  with the

inverse squared uncertainties as weightings. We chose the base functions  $f_1$  and  $f_2$  to be the difference between the hyperfine frequency splittings from the dipole and quadrupole

TABLE II. Measured absolute transition frequencies between the  $5S_{1/2}$  and  $6P_{1/2}$  states of  $^{85}\text{Rb}$  and  $^{87}\text{Rb}$  in comparison to the literature values given in Ref. [27].  $2\sigma$  uncertainties are given in brackets.

	Transition	Frequency [THz]	Literature [THz] [27]	difference [MHz]
$^{87}\text{Rb}$	$F = 2 \rightarrow F' = 1$	710.95797262(2000)	710.957977778(40)	5.158
	$F = 2 \rightarrow F' = 1/2$	710.95810595(2000)	710.958110355(50)	4.405
	$F = 2 \rightarrow F' = 2$	710.95823781(2000)	710.958242899(40)	5.089
$^{85}\text{Rb}$	$F = 3 \rightarrow F' = 2$	710.95924172(2000)	710.959248217(40)	6.497
	$F = 3 \rightarrow F' = 2/3$	710.95930044(2000)	710.959306912(40)	6.472
	$F = 3 \rightarrow F' = 3$	710.95935903(2000)	710.959365587(40)	6.557
$^{85}\text{Rb}$	$F = 2 \rightarrow F' = 2$	710.96227744(2000)	710.962283962(120)	6.522
	$F = 2 \rightarrow F' = 2/3$	710.96233612(2000)	710.962342621(80)	6.501
	$F = 2 \rightarrow F' = 3$	710.96239475(2000)	710.962401328(80)	6.578
$^{87}\text{Rb}$	$F = 1 \rightarrow F' = 1$	710.96480730(2000)	710.964812509(140)	5.209
	$F = 1 \rightarrow F' = 1/2$	710.96493983(2000)	710.964944993(80)	5.163
	$F = 1 \rightarrow F' = 2$	710.96507249(2000)	710.965077596(80)	5.106

TABLE III. Hyperfine splitting and hyperfine shifts.  $2\sigma$  uncertainties are given in brackets.

Transition $^{85}\text{Rb}$	Literature [MHz]	Frequency [MHz]
$6P_{1/2} F = 2 - F = 3$	117.368(100) [27]	117.33(66)
$6P_{1/2}$ hyperfine shift	73.345(170) [27]	73.32(42)
$6P_{3/2} F = 1 - F = 2$	9.806(32) [19]	9.802(25)
$6P_{3/2} F = 2 - F = 3$	20.852(84) [19]	20.850(24)
$6P_{3/2} F = 3 - F = 4$	39.268(124) [19]	39.265(23)
$6P_{3/2}$ hyperfine shift	32.719(54) [19]	32.716(16)
Transition $^{87}\text{Rb}$	Frequency [MHz]	Frequency [MHz]
$6P_{1/2} F = 1 - F = 2$	265.104(104) [27]	265.12(66)
$6P_{1/2}$ hyperfine shift	154.640(154) [27]	154.65(39)
$6P_{3/2} F = 0 - F = 1$	23.747(58) [19]	23.744(28)
$6P_{3/2} F = 1 - F = 2$	51.447(84) [19]	51.445(25)
$6P_{3/2} F = 2 - F = 3$	87.053(112) [19]	87.050(23)
$6P_{3/2}$ hyperfine shift	63.313(54) [19]	63.311(14)

expectation values of the associated Hamiltonians. Crossover transitions are handled by taking the average splitting of both contributing substates. The resulting values are listed in Table IV for both isotopes and are in good agreement with the literature data. For better comparability to the literature values, the values are given with  $1\sigma$  uncertainties here.

Figure 9 compares the results for the magnetic dipole and the electric quadrupole constant for the  $5S \rightarrow 6P_{3/2}$  transition of  $^{85}\text{Rb}$  and  $^{87}\text{Rb}$  with the literature values from Refs. [19,25,28,29] for  $^{87}\text{Rb}$  and  $^{85}\text{Rb}$ . The total isotope shifts are 41.935(60) MHz for the  $6P_{3/2}$  isotopes and 41.237(63) MHz for the  $6P_{1/2}$  isotopes, which also agree well with the literature values [21,22].

## VI. CONCLUSION

In summary, we have performed high-precision saturated absorption spectroscopy of  $^{85}\text{Rb}$  and  $^{87}\text{Rb}$  using a diode laser. The laser was stabilized and scanned by a wavelength meter for the  $6P_{1/2}$  transition and locked to a narrow linewidth fre-

quency comb for the  $6P_{3/2}$  transition. This allows for absolute frequency measurements with a  $2\sigma$  uncertainty of  $\leq 20$  kHz for the  $6P_{3/2}$  transition and  $\leq 20$  MHz for the  $6P_{1/2}$  transition. The lower uncertainty in the measurement of the  $5S \rightarrow 6P_{3/2}$  transition results from the laser locking to a frequency comb, while for the measurement of the  $5S \rightarrow 6P_{1/2}$  transition it is limited by the absolute uncertainty of the wavelength meter. From the measured data we derive transition frequencies for the  $5S \rightarrow 6P_{3/2}$  transition with unprecedented accuracy and verify the literature values for the hyperfine splitting, isotope shifts, the magnetic dipole constant, and the electric quadrupole constant.

## ACKNOWLEDGMENTS

This work has been supported by the DFG (SSP 1929 GiRyd and DFG FO740/4-1) and BMBF (FKZ: 13N14903) as well as the DLR Space Administration with funds provided by the Federal Ministry for Economic Affairs and Energy (BMWi) under Grant No. 50WM1857. The authors acknowledge additional support from the Evangelisches Studienwerk Villigst e.V.

TABLE IV. Calculated values for the magnetic dipole constant  $A$  and the electric quadrupole constant  $B$ .  $1\sigma$  uncertainties are given in brackets.

Transition	Constant	Literature [MHz]	This work [MHz]
$^{85}\text{Rb } 5S \rightarrow 6P_{3/2}$	A	8.179(12) [19]	8.1667(94)
$^{85}\text{Rb } 5S \rightarrow 6P_{3/2}$	B	8.190(49) [19]	8.126(54)
$^{87}\text{Rb } 5S \rightarrow 6P_{3/2}$	A	27.700(17) [19]	27.710(15)
$^{87}\text{Rb } 5S \rightarrow 6P_{3/2}$	B	3.953(24) [19]	4.030(42)
$^{85}\text{Rb } 5S \rightarrow 6P_{1/2}$	A	39.132(99) [27]	39.470(32)
$^{87}\text{Rb } 5S \rightarrow 6P_{1/2}$	A	132.552(94) [27]	133.24(28)

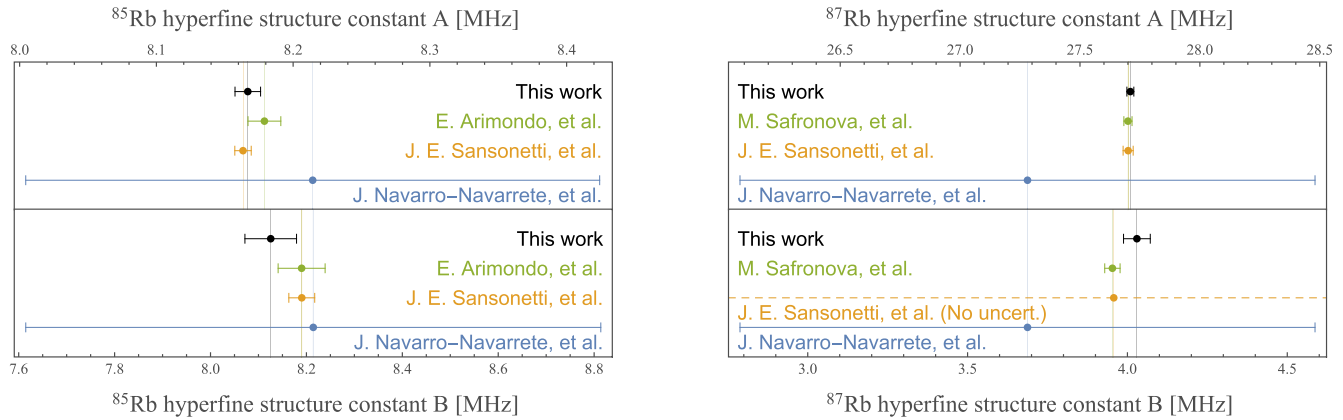


FIG. 9. Comparison of the determined values for the  $A$  and  $B$  constants for the  $5S \rightarrow 6P_{3/2}$  transition of  $^{85}\text{Rb}$  and  $^{87}\text{Rb}$ , respectively. The error bars are given as  $1\sigma$  uncertainties.

[1] T. Udem, R. Holzwarth, and T. W. Hänsch, *Nature (London)* **416**, 233 (2002).

[2] T. Udem, R. Holzwarth, and T. Hänsch, *Eur. Phys. J.: Spec. Top.* **172**, 69 (2009).

[3] S. T. Cundiff and J. Ye, *Rev. Mod. Phys.* **75**, 325 (2003).

[4] Y.-J. Huang, Y.-C. Guan, Y.-C. Huang, T.-H. Suen, J.-L. Peng, L.-B. Wang, and J.-T. Shy, *Phys. Rev. A* **97**, 032516 (2018).

[5] W.-K. Lee and H. S. Moon, *Phys. Rev. A* **92**, 012501 (2015).

[6] M. Saffman, T. G. Walker, and K. Mølmer, *Rev. Mod. Phys.* **82**, 2313 (2010).

[7] H. Levine, A. Keesling, A. Omran, H. Bernien, S. Schwartz, A. S. Zibrov, M. Endres, M. Greiner, V. Vuletić, and M. D. Lukin, *Phys. Rev. Lett.* **121**, 123603 (2018).

[8] K. R. Patton and U. R. Fischer, *Phys. Rev. Lett.* **111**, 240504 (2013).

[9] L. Sárkány, J. Fortágh, and D. Petrosyan, *Phys. Rev. A* **92**, 030303(R) (2015).

[10] M. Mack, F. Karlewski, H. Hattermann, S. Höckh, F. Jessen, D. Cano, and J. Fortágh, *Phys. Rev. A* **83**, 052515 (2011).

[11] C. Simonelli, M. Archimi, L. Asteria, D. Capocchi, G. Masella, E. Arimondo, D. Ciampini, and O. Morsch, *Phys. Rev. A* **96**, 043411 (2017).

[12] R. Gutiérrez, C. Simonelli, M. Archimi, F. Castellucci, E. Arimondo, D. Ciampini, M. Marcuzzi, I. Lesanovsky, and O. Morsch, *Phys. Rev. A* **96**, 041602(R) (2017).

[13] E. Gomez, S. Aubin, L. A. Orozco, and G. D. Sprouse, *J. Opt. Soc. Am. B* **21**, 2058 (2004).

[14] L. Sárkány, J. Fortágh, and D. Petrosyan, *Phys. Rev. A* **97**, 032341 (2018).

[15] D. A. Steck,  $^{87}\text{Rb}$  d line data, 2001.

[16] W. Li, I. Mourachko, M. W. Noel, and T. F. Gallagher, *Phys. Rev. A* **67**, 052502 (2003).

[17] J. Han, Y. Jamil, D. V. L. Norum, P. J. Tanner, and T. F. Gallagher, *Phys. Rev. A* **74**, 054502 (2006).

[18] K. Afrousheh, P. Bohlouli-Zanjani, J. A. Petrus, and J. D. D. Martin, *Phys. Rev. A* **74**, 062712 (2006).

[19] E. Arimondo, M. Inguscio, and P. Violino, *Rev. Mod. Phys.* **49**, 31 (1977).

[20] K. Enomoto, N. Hizawa, T. Suzuki, K. Kobayashi, and Y. Moriwaki, *Appl. Phys. B* **122**, 126 (2016).

[21] P. Grundevik, M. Gustavsson, A. Rosén, and S. Svanberg, *Z. Phys. A: At. Nucl.* **283**, 127 (1977).

[22] L. Aldridge, P. L. Gould, and E. E. Eyler, *Phys. Rev. A* **84**, 034501 (2011).

[23] J. Ye, S. Swartz, P. Jungner, and J. L. Hall, *Opt. Lett.* **21**, 1280 (1996).

[24] R. W. P. Drever, J. L. Hall, F. V. Kowalski, J. Hough, G. M. Ford, A. J. Munley, and H. Ward, *Appl. Phys. B* **31**, 97 (1983).

[25] M. S. Safronova and U. I. Safronova, *Phys. Rev. A* **83**, 052508 (2011).

[26] HighFinesse GmbH, Datasheet WS8-2 (available under [www.highfinesse.com](http://www.highfinesse.com) 2020).

[27] A. Shiner, A. Madej, P. Dubé, and J. Bernard, *Appl. Phys. B* **89**, 595 (2007).

[28] J. E. Sansonetti, *J. Phys. Chem. Ref. Data* **35**, 301 (2006).

[29] J. Navarro-Navarrete, A. Díaz-Calderón, L. Hoyos-Campo, F. Ponciano-Ojeda, J. Flores-Mijangos, F. Ramírez-Martínez, and J. Jiménez-Mier, [arXiv:1906.07114](https://arxiv.org/abs/1906.07114).